Copyright WILEY-VCH Verlag GmbH & Co. KGaA, 69469 Weinheim, Germany, 2013.

ADVANCED FUNCTIONAL MATERIALS

Supporting Information

for *Adv. Funct. Mater.*, DOI: 10.1002/adfm.201303180

Efficient Si Nanowire Array Transfer via Bi-Layer Structure Formation Through Metal-Assisted Chemical Etching

*Taeho Moon, Lin Chen, Shinhyun Choi, Chunjoong Kim, and Wei Lu**

Submitted to ADVANCED FUNCTIONAL MATERIALS

Supporting Information

Efficient Si Nanowire Array Transfer via Bi-Layer Structure Formation through Metal-Assisted Chemical Etching

Taeho Moon[1], Lin Chen[1], Shinhyun Choi[1], Chunjoong Kim[2], and Wei Lu[1,*]

[1]Department of Electrical Engineering and Computer Science,
the University of Michigan, Ann Arbor, MI 48109
[2]Lawrence Berkeley National Laboratory, Berkeley, CA 94720-8168

To gain insight on how the bilayer structure formation can facilitate NW breakage and transfer, a control experiment was performed in which the sample with 90 min etch time was dried naturally overnight (i.e. without critical point drying) after water rinsing. The results are shown in Fig. S1. Generally, vertical NWs will experience significant bundling upon drying in air due to the surface tension exerted on the NWs during the evaporation of liquid.[1] In this case, breakage of the top-layer SiNWs from the bottom layer is clearly observed at the interface, and cracks are observed at the bilayer interface and also at specific heights in the bottom layer. The crack formation at the bilayer interface is likely caused by the strong surface tension during water evaporation, and similar effects can explain why better NW breakage and transfer yield can be obtained in samples with well-defined bilayer structures. These lateral damages in turn produce the horizontal cracks when experienced with shear force, as in the cases of contact printing or liquid evaporation. Assuming the bottom columns have cylindrical shape with the average diameter of ~3 um (Fig. S1), the number of NWs branched from a single bottom column can be roughly estimated to ~700, for the Au-mesh-pore periodicity of 107 nm.

The effects of Au-mesh geometries on the etching-morphology evolution were summarized in Fig. S2 for different etching times, showing the total etch thickness, the top-layer NW thickness, and the bottom-layer thickness, respectively. The regions exhibiting bilayer structures were highlighted as the pink-shaded areas through extrapolations considering the tendencies of the bottom-layer thicknesses. With the increase of Au-mesh periodicity, a few phenomena can be observed such as the increase of total etching rate, the overall increase of top-layer NW thickness, and the retardation of the bi-layer structure formation. The geometry dependence on etching morphology suggests that mass transport plays a key role in the bilayer structure formation, as diffusion becomes easier with the increase of Au-mesh periodicity. The exact mass-transport mechasnim of how the etching can proceed at the microscopic scale is still under debate when contiguous metal films are used as catalyst. In this study we adopt a mass-transport model proposed by N. Geyer *et*. al which states that a thin porous layer is first created in the Si layer underneath the metal film; followed by the diffusion of the etching reagent and the byproduct through the porous layer towards the openings of the film (i.e. the edge of the Au dots). Repeating this process leads to Si dissolution and the vertical movement of the metal catalyst film into the Si substrates.[2] This model seems most plausible among possible diffusion models during MaCE to our best knowledge. According to this model, in our case, two effects on diffusion paths are expected with increasing Au-mesh-pore periodicity, such as the improvement in diffusion between the bulk electrolyte and the Au/Si interface and the increased distance for the diffusion through the porous layer under the Au film [Fig. S3]. The competition between these two processes suggests the aspect ratio of the etched pores is likely the limiting factor for the mass transport and the position of the uniform horizontal border is determined by the critical aspect ratio.

References

[1] H. Han, J. Kim, H. S. Shin, J. Y. Song, W. Lee, *Adv. Mater*. **2012**, *24*, 2284.

[2] N. Geyer, B. Fuhrmann, Z. Huang, J. Boor, H. S. Leipner, P. Werner, *J. Phys. Chem. C* **2012**, *116*, 13446.

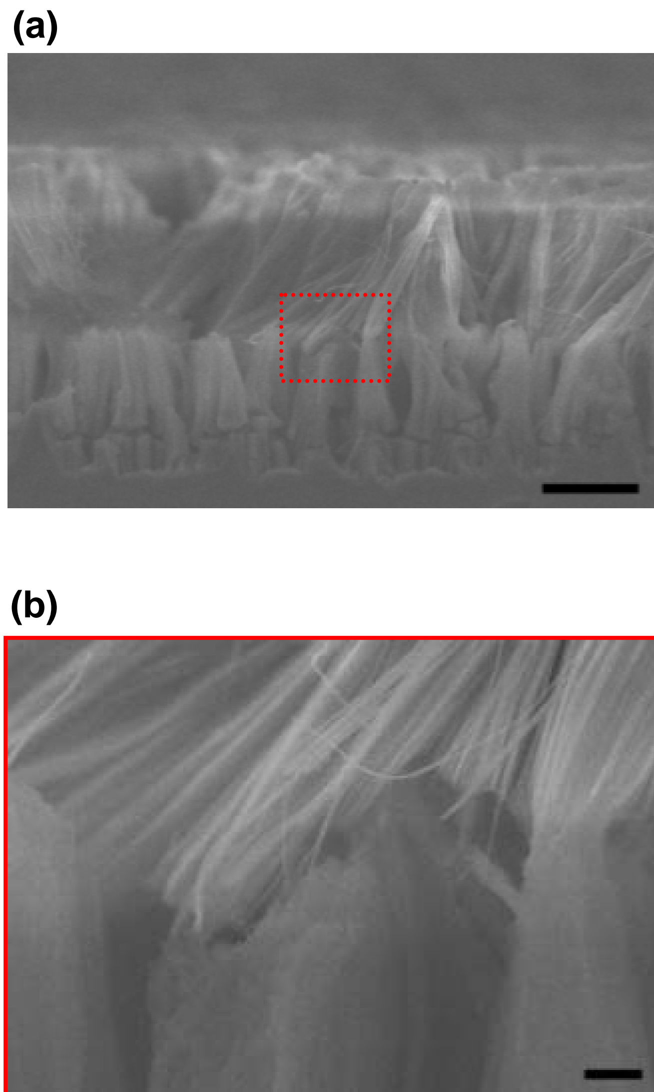

Figure S1. Confirmation of horizontal cracks formed with bi-layer structure, in a control sample experienced natural drying. (a) SEM image of the naturally overnight-dried sample (etched for 90 min), without critical point drying. Scale bar: 10 μm. (b) Magnified image of (a) in the middle showing the crack formation at the bilayer interface. Scale bar: 1 μm.

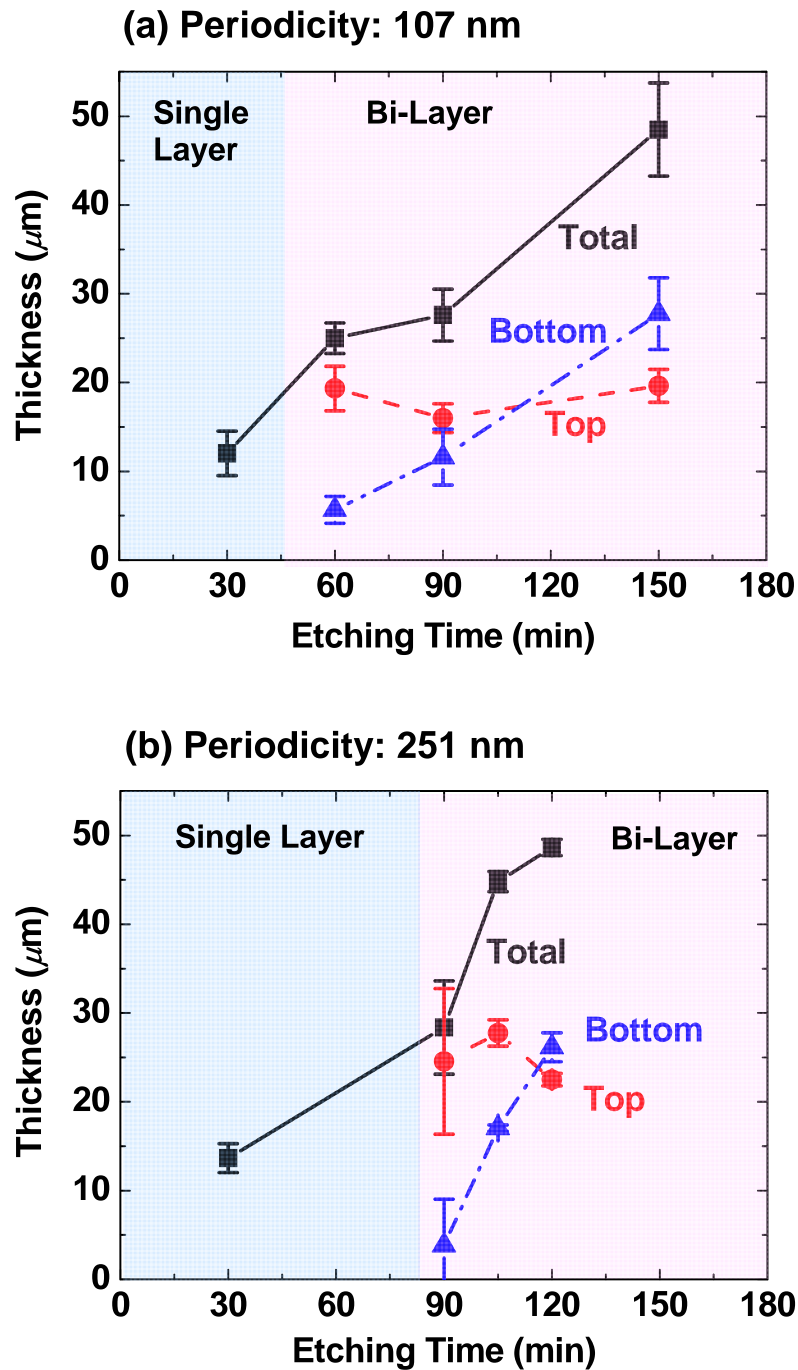

Figure S2. Comparison of etching-morphology evolution with different Au-mesh geometries. Etching-time dependences of total thickness (black), top-layer thickness (red), and bottom-layer thickness (blue) were plotted for Au-mesh-pore periodicities of (a) 107 nm and (b) 251 nm. The pink shaded areas highlight the etching conditions that exhibit clear bi-structure.

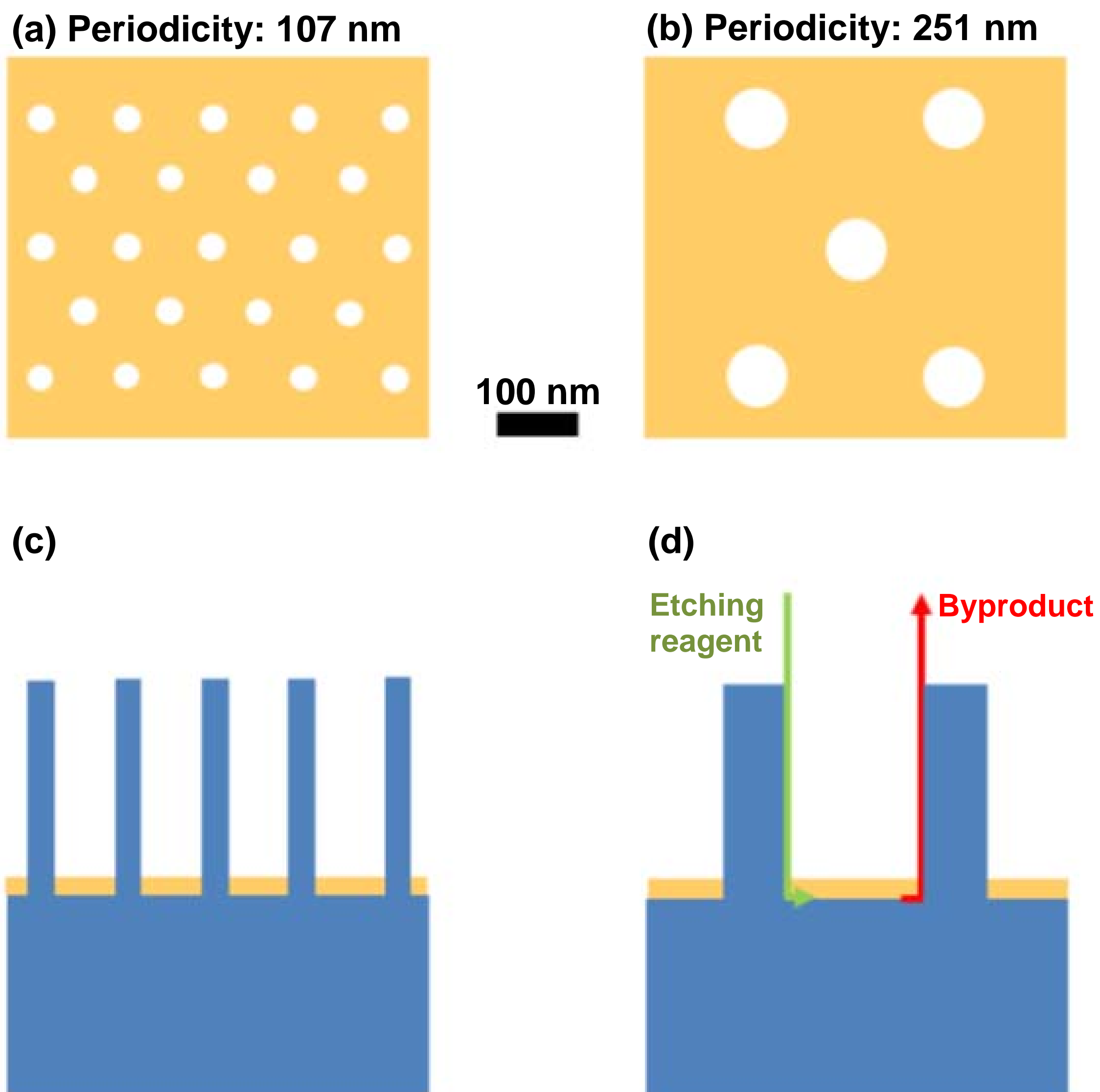

Figure S3. Schematic illustrations showing the effects of Au-mesh geometries on diffusion during MaCE. (a-b) Au meshes following the AAO geometries with the pore periodicities (diameters) of 107 nm (35 nm) and 251 nm (80 nm). (c-d) Differences of diffusion path during MaCE, according to Au-mesh geometries.

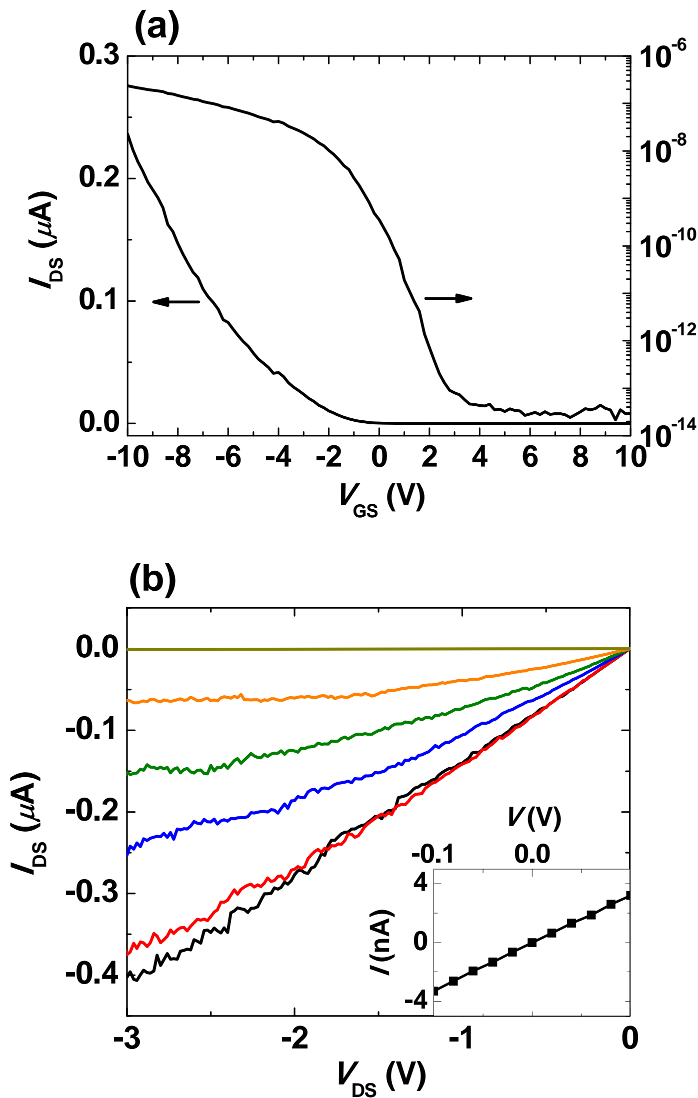

Figure S4. Single NW FETs fabricated by using wet transfer. (a) V_{GS}-I_{DS} curves with V_{DS} = -1 V (left: linear scale, right: log scale). (b) V_{DS}-I_{DS} family curves. V_{GS} = -10 to 0 V in 2 V steps from bottom to top. Inset: V_{DS}-I_{DS} curve at low voltage showing ohmic behavior with Au contacts.